

# High temperature oxidation and compressive strength of Cr<sub>2</sub>AlC MAX phase foams with controlled porosity

J. Gonzalez-Julian,<sup>1\*</sup> S. Onrubia,<sup>1</sup> M. Bram,<sup>1</sup> C. Broeckmann,<sup>2</sup> R. Vassen,<sup>1</sup> and O. Guillon<sup>1</sup>

<sup>1</sup> Forschungszentrum Jülich GmbH, Institute of Energy and Climate Research: Materials Synthesis and Processing (IEK-1), 52425 Jülich, Germany.

<sup>2</sup> Institute for Materials Applications in Mechanical Engineering (IWM), RWTH Aachen University, Augustinerbach 4, 52062 Aachen, Germany.

\* Corresponding author

## Abstract

Cr<sub>2</sub>AlC foams have been processed for the first time containing low (35 vol.%), intermediate (53 vol.%) and high (75 vol.%) content of porosity and three ranges of pore size, 90 – 180 µm, 180 – 250 µm and 250 - 400 µm. Sacrificial template technique was used as processing method, utilizing NH<sub>4</sub>HCO<sub>3</sub> as temporary pore former. Cr<sub>2</sub>AlC foams exhibited negligible oxidation up to 800 °C and excellent response up to 1300 °C due to the *in-situ* formation of an outer thin continuous protective layer of α-Al<sub>2</sub>O<sub>3</sub>. The *in-situ* α-Al<sub>2</sub>O<sub>3</sub> protective layer covered seamlessly all the external surface of the pores, even when they present sharp angles and tight corners, reducing significantly the further oxidation of the foams. The compressive strength of the foams was 73 and 13 MPa for 53 vol.% and 75 vol.% porosity, respectively, which increased up to 128 and 24 MPa after their oxidation at 1200 °C for 1 hour. The increase in the compressive strength after the oxidation was caused by the switch from inter- to transgranular fracture mode. According to the excellent high temperature response, heat exchangers and catalyst supports are the potential application of these foams.

## 1. Introduction

Ceramic foams present unique features for several engineering applications that cannot be achieved by their conventional dense counterparts, attracting large interest from industry and scientific community.<sup>1</sup>

The industrial attention on these reticulated structures is caused by the combination of the ceramic properties with the functionality of the porous substrates. As ceramic materials, they exhibit high melting point, and good oxidation and corrosion resistances at high temperatures, while as a porous material they present high surface area, controlled permeability, low density, high specific strength and low thermal mass. According to these features, the final porous components typically operate under harsh environments of high temperature and flux of corrosive atmospheres/materials such as filters for exhaust gases, particles or molten metals. Furthermore, they can be used as supports for catalytic reactions and membranes. However, ceramic components are brittle, effect that is strongly magnified in reticular structures by the porosity, limiting the industrial spread of the ceramic foams. The lack of enough mechanical stability has generated the use of metallic alloys as porous substrates in many applications, despite their lower oxidation and corrosion resistances. This limits the operating temperature of the systems, i.e. in heat exchangers, where carbon steel and stainless steel should not exceed 425 and 650 °C, respectively.<sup>2</sup> Furthermore, due to the high corrosion of the metallic components, the whole process has to be regularly stopped to replace the eroded parts, reducing the efficiency and increasing the costs. In that sense, one of the most promising alternatives to solve both problems – brittleness of components and oxidation/corrosion resistance – is to use porous structures based on MAX phase compounds.

MAX phases are a relative new family of material, where M is an early transition metal, A corresponds with an A-group element (IIIA or IVA element) and X is C or N.<sup>3</sup> Currently, more than 70 different MAX phases have been discovered and the number of new phases described in the literature increases every year. Nevertheless, the main interest on MAX phases resides in their unique combination of properties, bridging the gap between metal and ceramic materials.<sup>4</sup> This peculiar response is caused by the combination of ionic/covalent and metallic bonding in the crystal structure. Due to their ceramic character, they present low density, high elastic modulus and good oxidation and corrosion resistance at

high temperature, whereas as their metal character, they exhibit high electric and thermal conduction, readily machinability, good thermal shock and damage tolerance.<sup>5</sup> Furthermore, MAX phases have an intermediate coefficient of thermal expansion and some of them show self-healing mechanisms at high temperature.<sup>6,7</sup> Among all the MAX phases,  $\text{Ti}_3\text{SiC}_2$ ,  $\text{Ti}_2\text{AlC}$  and  $\text{Ti}_3\text{AlC}_2$  have been the most studied compounds due to their combination of properties, although in terms of high temperature applications,  $\text{Cr}_2\text{AlC}$  is one of the most interesting phases because of its excellent oxidation resistance at high temperature in air (oxidation rate of  $1.1 \cdot 10^{-11}$  and  $3.0 \cdot 10^{-9} \text{ kg}^2\text{m}^{-4}\text{s}^{-1}$  at 1000 and 1300 °C, respectively).<sup>8</sup> Consequently, the main advantages of MAX phases over the conventional porous ceramics are the better mechanical response – higher fracture toughness, damage tolerance and thermal shock -, the easily machining of intricate parts, and the high electrical conduction, maintaining the good oxidation and corrosion resistances of the advanced ceramics. The higher fracture toughness, as well as the good thermal shock and damage tolerance, can overcome the problem of the mechanical stability of foams, while the easily machining reduce costs and facilitate the transfer of final complex components to industrial applications. In that sense, electrical discharge machining (EDM) can be used due to the high electrical conduction of the MAX phases. Furthermore, the electrical conduction can be determinant in specific applications such as catalytic converters. For example, the high-efficient catalytic converters in automotive are electrically heated during the cold start of the engine, where the 50%-90% of the total emission of hydrocarbons are released to the atmosphere.<sup>9,10</sup> Unfortunately, ceramic catalyst supports, such as  $\text{Al}_2\text{O}_3$ , SiC or mullite cannot be used for this application due to their insulating nature, using Fe-Cr-Al alloys as the only alternative. On the other hand, the advantageous of use MAX phase instead superalloys is the increase of the maximal working temperature ( $> 1100$  °C) by the better oxidation and corrosion resistance, with the consequent rise of the energy efficiency and the longer durability of components. Furthermore, MAX phases do not contain hazardous and limited elements, whereas they are typically required for high temperature superalloy compounds.<sup>11</sup>

Ceramic porous materials have been widely investigated during the last decades due to their high industrial interest.<sup>12,1</sup> In general, there are three main routes to produce reticulate structures with controlled porosity: i) replica method, ii) sacrificial template and iii) direct foaming. However, porous structures based on MAX phases have been just slightly investigated so far, focusing only on  $\text{Ti}_2\text{AlC}$ ,  $\text{Ti}_3\text{AlC}_2$  and  $\text{Ti}_3\text{SiC}_2$  between more than 70 known MAX phase compounds.<sup>13</sup> Sun et al.<sup>14</sup> reported the first intentioned porous  $\text{Ti}_3\text{SiC}_2$  through the incomplete densification process, although this process does not allow tailoring the porosity. Nevertheless, the mechanical characterization showed the high potential of these structures due to the fully reversible and closed hysteresis loops of deformation under subsequent cycles of compression. Sacrificial template method has been successfully used to obtain porous  $\text{Ti}_2\text{AlC}$  using either NaCl or raw sugar by Hu<sup>15</sup> and Velasco<sup>16</sup>, respectively. The obtained  $\text{Ti}_2\text{AlC}$  foams vary between 10 and 80 vol. % of porosity and between 42 to 1000  $\mu\text{m}$  in porous size. In addition,  $\text{Ti}_2\text{AlC}$  porous structures have been also performed by replica method by Bowen et al.<sup>17</sup>. The potential application of these  $\text{Ti}_2\text{AlC}$  foams is to produce electrically conductive electrodes for harsh environments or microbial fuel cells. Sun et al.<sup>18</sup> reported the production of  $\text{Ti}_3\text{AlC}_2$  foams using the replica method as well. The reticulated structures presented 80 vol.% of open porosity with well-defined and homogeneous porosity after removing the sponge template. The  $\text{Ti}_3\text{AlC}_2$  reticulated structures were used as catalyst supports for high-efficient gas exhaust systems, growing nanocrystalline  $\text{CeO}_2$  coatings on the surface of the porous structures by a cathodic electrogeneration method. Potoczek et al.<sup>19</sup> developed  $\text{Ti}_2\text{AlC}$  foams with high porosity, up to 93 vol.%, and a high degree of interconnectivity between them by gel casting using agarose. The average cell size ranged from 335 to 615  $\mu\text{m}$ , and the average cell window size from 72 to 162  $\mu\text{m}$  for 87 and 93 vol.% porosity, respectively. The number of possible applications is high despite the small number of reported works, confirming the interest and potential of these porous MAX phases. However, to transfer porous MAX phases to final applications two aspects have to be confirmed: i) testing at high temperature of the foams, and ii) processing of

porous structures based on other MAX phases with excellent response at high temperature, which is expected for example in the case of  $\text{Cr}_2\text{AlC}$ . The processing of  $\text{Cr}_2\text{AlC}$  foams might be interesting for different applications, such as heat exchangers and/or catalyst supports, due to the high thermal and electrical conductivity of this MAX phase in combination with the excellent resistance to harsh environment at high temperatures.<sup>2</sup>

The aim of the current work is to develop for the first time porous  $\text{Cr}_2\text{AlC}$  structures, testing their oxidation resistance up to 1300 °C in air and the compressive strength before and after the oxidation. Sacrificial template method using ammonium hydrogen bicarbonate ( $\text{NH}_4\text{HCO}_3$ ) as temporary space holders was selected due to its versatility to process low and high porous materials with high range of pore sizes. The developed materials contained porosity up to 75 vol. % with three different ranges of porous size, 90-180  $\mu\text{m}$ , 180-250  $\mu\text{m}$ , and 250-400  $\mu\text{m}$ .

## **2. Experimental procedure**

$\text{Cr}_2\text{AlC}$  pure powder was synthesized from their elemental constituents by solid-liquid state reaction at high temperature. The synthesis process and the evolution of the different phases with the temperature are described elsewhere.<sup>20</sup> In summary, chromium (-100 mesh,  $d_{50} = 85.5 \mu\text{m}$ , 99.0% pure), aluminum (-325 mesh,  $d_{50} = 9.1 \mu\text{m}$ , 99.5% pure) and graphite ( $d_{50} = 6.9 \mu\text{m}$ , 99.0% pure) powders (all from Alfa Aesar, Germany) were used as starting materials. First, the chromium powder was milled using planetary milling (PM400, Retsch, Germany) with Cr-alloy balls (5 mm diameter) for 3h at 400 r.p.m. under argon atmosphere to avoid oxygen contamination. The milled chromium particle size distribution was unimodal with  $d_{10} = 9.9 \mu\text{m}$ ,  $d_{50} = 26.4 \mu\text{m}$  and  $d_{90} = 64.7 \mu\text{m}$ . Afterwards, the powders were weighed according to the desired composition (Cr : Al : C = 2.0 : 1.1 : 1.0). An extra 10 at.% of aluminum was added to compensate its loss during the synthesis process at high temperature. The powders were mixed using planetary milling for 20 min at 150 r.p.m. under argon atmosphere. Then, the resultant

mixed powder was uniaxially pressed at 200 MPa and heat treated under argon atmosphere to synthesize the  $\text{Cr}_2\text{AlC}$  phase. The heat treatment was carried out at  $5^\circ\text{C}/\text{min}$  up to  $1400^\circ\text{C}$  and isothermal holding time of 3 h. The synthesized  $\text{Cr}_2\text{AlC}$  samples were ground in an agate mortar and vibrational milled (Pulverisette Spartan, Fritsch, Germany), obtaining the final  $\text{Cr}_2\text{AlC}$  powder with an unimodal particle size distribution ( $d_{10} = 4.6\ \mu\text{m}$ ,  $d_{50} = 9.2\ \mu\text{m}$  and  $d_{90} = 16.8\ \mu\text{m}$ ). Ammonium hydrogen bicarbonate ( $\text{NH}_4\text{HCO}_3$ , Alpha Aesar, Germany) was used as temporary space holder material.  $\text{NH}_4\text{HCO}_3$  powder was sieved to separate three different ranges of particle sizes:  $90 - 180\ \mu\text{m}$ ,  $180 - 250\ \mu\text{m}$  and  $250 - 400\ \mu\text{m}$ . The content of the space holder was 40, 60 and 80 vol. % referred to the  $\text{Cr}_2\text{AlC}$  powder, so 9 different compositions were prepared.  $\text{Cr}_2\text{AlC}$  and  $\text{NH}_4\text{HCO}_3$  powders were mixed until the complete homogenization, followed by cold uniaxial pressing at 200 MPa. The result cylinders presented 13 mm diameter and 10 mm height. The space holders were eliminated from the green bodies before the sintering process by a thermal process at low temperature. Therefore, the samples were placed into an open air furnace and heated at  $1^\circ\text{C}/\text{min}$  up to  $80^\circ\text{C}$  for 10 hours. Finally, the porous compacts were consolidated at  $1250^\circ\text{C}$  for 5 hours under argon atmosphere. In addition, pure  $\text{Cr}_2\text{AlC}$  samples without space holders were consolidated following the whole previous processing route as blank specimens.

Density of the samples was measured by Archimedes method in water at room temperature. Specimens were ground and polished up to  $0.5\ \mu\text{m}$  diamond paste for the microstructure and pore characterization. Polished surfaces were observed in a tabletop scanning electron microscope (TM3030 Hitachi, Japan), whereas the fracture surfaces were observed in a scanning electron microscope (SEM, Zeiss Ultra55, Germany) for the microstructural characterization.

The analysis of the oxidation response of the  $\text{Cr}_2\text{AlC}$  compounds was carried out in two steps. First, thermogravimetric analysis (TGA, Netzsch STA 449, Germany) was carried out on the blank specimens to define the oxidation temperatures. TGA studies were carried out from room temperature to  $1300^\circ\text{C}$

under synthetic dry air, heating at 10 °C/min and 1 h of isothermal holding time. In a second step and according to the information obtained from the TGA analysis, porous and blank specimens were oxidized under synthetic air at maximal temperature of 800 °C, 900 °C, 1000 °C, 1100 °C, 1200 °C and 1300 °C, using for all these temperatures the same heating rate and dwell time, 10 °C/min and 1h, respectively. Oxidized surfaces were analyzed by X-ray diffraction (XRD, D8-Discover, Bruker). After that, samples were perpendicularly cut, ground and polished in order to observe the cross section and the different oxidized layers using a tabletop microscope. The observed areas were located in the middle of the samples with at least few mm from the outer surface of the sample in order to analyze the oxidation in the core of the porous structures. In addition, chemical analysis of the different layers was carried out using energy-dispersive spectroscopy (EDS) unit included in the tabletop microscope. Compressive tests were performed at room temperature using a universal testing machine (Instron) under displacement control mode at a crosshead speed of 0.018 mm/s. Cr<sub>2</sub>AlC samples with 53 vol.% and 75 vol.% of porosity and pore size between 180 and 250 µm were tested. Samples were machined by EDM in cylinders with diameter of 6.5 mm and height of 9.0 mm. Half of the samples were tested (no oxidation) and the rest were oxidized at 1200 °C during 1 hour prior to the mechanical testing. At least 6 samples were tested per condition. Fracture surfaces after the compressive tests of the Cr<sub>2</sub>AlC foams with 53 vol.% of porosity with and without oxidation treatment were observed in the SEM.

### **3. Results and discussion**

#### **3.1. Processing of Cr<sub>2</sub>AlC foams**

Characterization of the synthesized starting Cr<sub>2</sub>AlC powder by XRD and SEM is shown in Figure 1. XRD patterns of the powder shows only Cr<sub>2</sub>AlC phase without any additional peak from the reactants or intermediate products during the synthesis process, indicating a highly pure Cr<sub>2</sub>AlC powder (Fig. 1a). The particles presented irregular shape and no obvious agglomerates were observed (Fig. 1b). At higher

magnifications, the characteristic layered structure of the MAX phases can be easily observed in the powder, as it is shown in Figure 1c. This highly pure and unimodal  $\text{Cr}_2\text{AlC}$  powder was mixed with the space holders, and sintered to consolidate the porous structures. Figure 2 shows the overall porosity of the consolidated samples as a function of the added space holder content for the three different ranges of pore sizes. Samples without space holders cannot be fully densified through this sintering conditions, presenting a residual porosity of 11.5 vol.%. This effect is common for the MAX phase compounds, which typically require sintering techniques assisted by pressure to obtain full densification.<sup>21</sup> Regarding the samples with space holders, the final porosities of all the consolidated porous structures are in good agreement with the content of the space holders added. Values of the final porosity are lower than the amount of space holders, but the difference is always less than 8 vol. %. This reduction of the overall final porosity was caused by the shrinkage during the sintering process. As a result, porosities of 35 vol.%, 53 vol.% and 75 vol.% were achieved for content of space holders of 40 vol.%, 60 vol.% and 80 vol.%, respectively. Interestingly, the final porosity of the materials is just controlled by the content of the space holders, and no influence in the final porosity was observed by the three different range of the particle size of the space holders. Microstructure of the porous samples can be observed in Figure 3, where representative micrographs with three different contents of porosity and pore size are shown. The samples contain 35 vol.% (Fig. 3a), 53 vol.% (Fig. 3b) and 75 vol.% (Fig. 3c) of porosity with sizes between 90 and 180  $\mu\text{m}$ , 180 – 250  $\mu\text{m}$  and 250 – 400  $\mu\text{m}$ , respectively. Grey areas correspond with the  $\text{Cr}_2\text{AlC}$  matrix, whereas black zones are the pores. Two different kinds of pores can be observed: i) big pores with irregular shape generated by the space holders and ii) small porosity (few micrometers) produced due to the incomplete densification. The porosity is homogeneously distributed without any preferential orientation into the materials, even for the highest content of 80 vol. %. Figure 4 shows the fracture surface of the sample with 53 vol.% of porosity and sizes between 180 and 250  $\mu\text{m}$ . The homogeneous porosity is confirmed in Figure 4a, where also the connectivity between pores is

observed. Pores were separated by  $\text{Cr}_2\text{AlC}$  struts with thicknesses between 10 to 60  $\mu\text{m}$ , which mostly contained few grains (Fig. 4b). As expected, each  $\text{Cr}_2\text{AlC}$  grain was composed by the characteristic nanolayered structure, which is observed in Figure 4c.

As a result,  $\text{Cr}_2\text{AlC}$  porous structures with low (35 vol.%), intermediate (53 vol.%) and high (75 vol.%) well-distributed porosity were successfully produced by the sacrificial template technique, using  $\text{NH}_4\text{HCO}_3$  as temporary material. This is the first time that  $\text{Cr}_2\text{AlC}$  foams with controlled porosity are developed, but microstructure and results are in concordance with the reported values of other MAX phases.<sup>17,22</sup> In these works,  $\text{Ti}_2\text{AlC}$  porous structures were obtained by sacrificial template as well, leading to porosities between 10 and 80 vol. % with pore sizes between 42 and 1000  $\mu\text{m}$ . Furthermore, good mechanical stability was reported,<sup>15,16</sup> although the foams contained lower porosity. As a main conclusion, sacrificial template is an excellent processing technique to develop MAX phase foams due to the flexibility in content and size of the porosity, and simplicity of the process.

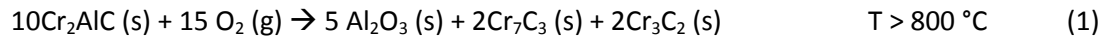
### **3.2. Oxidation response of $\text{Cr}_2\text{AlC}$ foams**

The oxidation behavior of the  $\text{Cr}_2\text{AlC}$  was firstly studied on samples produced without template (porosity  $\sim 11$  %) by thermogravimetric analysis in technical air from room temperature to 1300  $^\circ\text{C}$  and 60 min of isothermal holding time (Fig. 5). Remarkable oxidation of  $\text{Cr}_2\text{AlC}$  started around 800  $^\circ\text{C}$ , and from this temperature the weight gain increases due to the continuous formation of oxide scale. The weight gain was 2.5 wt.% up to 1300  $^\circ\text{C}$ , and only  $< 0.5$  wt.% during 60 min at the maximal temperature, indicating an excellent oxidation response at this temperature. According to this oxidation behavior,  $\text{Cr}_2\text{AlC}$  blank samples were oxidized at 800, 900, 1000, 1100, 1200 and 1300  $^\circ\text{C}$  with 1 h of isothermal holding time to analyze the microstructure evolution. The phase evolution was characterized by XRD on the sample surface after the oxidation tests (Fig. 6) and through the SEM observation of the polished cross sections of the oxidized specimens (Fig. 7). Firstly, it should be noted that  $\text{Cr}_2\text{AlC}$  is the only crystalline phase

presented in the sample after the consolidation process, so other phases detected after the oxidation treatment were formed during this event. At 800 °C only  $\text{Cr}_2\text{AlC}$  phase was observed, confirming the absence of notable oxidation at this temperature previously characterized by TGA (Fig. 5). The first clear peak related to oxidation was detected at 900 °C, which was  $\alpha\text{-Al}_2\text{O}_3$  (corundum phase). The intensity of the  $\alpha\text{-Al}_2\text{O}_3$  peaks was really low – just traces –, slightly increasing at 1000 °C. These results are also in concordance with the previous TGA results since the formation of oxidized specimens will increase the weight of the samples. Nevertheless, the major phase at this temperature was still  $\text{Cr}_2\text{AlC}$  with the presence of small peaks of  $\alpha\text{-Al}_2\text{O}_3$ . At 1100 °C, the  $\alpha\text{-Al}_2\text{O}_3$  peaks continued growing and the first small peaks of  $\text{Cr}_7\text{C}_3$  appeared. When the temperature was increased up to 1200 °C,  $\alpha\text{-Al}_2\text{O}_3$  and  $\text{Cr}_7\text{C}_3$  became the major phases. Besides, small amounts of  $\text{Cr}_3\text{C}_2$  phase were detected at this temperature. Finally, at 1300 °C, the presented phases on the surface were mainly  $\alpha\text{-Al}_2\text{O}_3$  and  $\text{Cr}_7\text{C}_3$  with small contents of  $\text{Cr}_3\text{C}_2$  and still some  $\text{Cr}_2\text{AlC}$  peaks from the starting material. According to these XRD results, polished cross sections of the samples oxidized at 1000, 1100, 1200 and 1300 °C were characterized in the SEM (Fig. 7). All the cross sections presented a similar structure: an outer and continuous grey layer over an intermediate white subscale, and beneath these two layers the  $\text{Cr}_2\text{AlC}$  bulk material. The only difference between the three samples is the thickness of the layers, which increases with the increment of temperature. Nevertheless, the thickness of both layers is just  $\sim 10\text{ }\mu\text{m}$  after 1 h at 1300 °C.

The external  $\alpha\text{-Al}_2\text{O}_3$  protective layer and the underneath carbide scale is formed as follows. At high temperature, around 800 °C (Fig. 5), aluminum atoms from the  $\text{Cr}_2\text{AlC}$  bulk structure preferred diffuse towards the surface, reacting subsequently with oxygen to form  $\alpha\text{-Al}_2\text{O}_3$ . The preferred diffusion of aluminum atoms is caused because of the singularity of the crystal structure of the  $\text{Cr}_2\text{AlC}$ , which is equal for all the MAX phases.<sup>3</sup> This crystal structure is based on  $\text{CrC}_6$  octahedras that are interleaved with layers of pure aluminum atoms. The bonding between Cr and Al is weaker than that between Cr and C, causing the preferred diffusion of the aluminum atoms out of the crystal structure. As a result,

aluminum reacts with the oxygen on the surface of the material, forming an outer layer of  $\alpha$ - $\text{Al}_2\text{O}_3$ . The deletion of aluminum creates an underneath layer based on chromium carbides. This intermediate carbide layer is composed by  $\text{Cr}_7\text{C}_3$  and  $\text{Cr}_3\text{C}_2$  phases (Fig. 6 and 7). The overall reaction of the oxidation process can be described as follows:



$\alpha$ - $\text{Al}_2\text{O}_3$  is well-known as protective layer against high-temperature corrosion in the presence of oxygen, so this thin layer is responsible of the excellent oxidation resistance of  $\text{Cr}_2\text{AlC}$  in air.<sup>8,23</sup> When the temperature is increased, the continuous external alumina layer grows causing the increase of the beneath carbide layer due to the migration of more aluminum atoms to the surface. Nevertheless, the oxide and the carbide layers are relative thin, with approx. 10  $\mu\text{m}$  of thickness in total after 1 h at 1300  $^\circ\text{C}$ . The composition of the layers was confirmed by the combination of XRD and EDS analysis on the sample oxidized at 1300  $^\circ\text{C}$  (Fig. 8). The outer layer is based on aluminum (Fig. 8b), whereas the intermediate layer is composed on Cr, whereas Al was not detected (Fig. 8c) in this layer. The bulk material contains Cr and Al, and corresponds with the non-oxidized  $\text{Cr}_2\text{AlC}$  compound.

The above microstructural characterization was carried out on samples produced without templates and flat surfaces, meanwhile porous structures present different features such as irregular and curved surfaces, which can affect the oxidation resistance by spallation of the protective layers and/or closing the connectivity between pores due to the formation of outer layers. Figure 9 shows representative cross sections in the center (at least few mm from the nearest external surface) of different porous samples oxidized at 1000, 1100 and 1300  $^\circ\text{C}$ . Similar results in terms of composition and thickness of the oxide layers were observed for both, the samples without space holders and porosity of 11 vol.% (Fig. 7) and the porous structures (Fig. 9) at the same temperature. All the pores exhibited the same oxidation behavior, showing good connectivity between pores after the oxidation treatment. Interestingly, as the

$\alpha$ -Al<sub>2</sub>O<sub>3</sub> was *in-situ* formed, it covered seamlessly all the external surface of the pores, even when they present sharp angles and tight corners, avoiding the further oxidation of the foams. This fact is critical as the irregular pore shapes contain sharp angles and tight corners, which could generate gaps between the layers promoting the inward diffusion of oxygen. Besides the seamless protection, the adhesion between the layers plays also a critical role. The bonding between the layers seems to be good, since no spallation and/or cracks have been detected. Furthermore, the porous structures perfectly maintain the mechanical stability, as well as the connectivity between them up to 1300 °C, so the surrounded air can continuously flowing through the foams. It has to be mentioned that the thickness of the oxide scales, and the consequent oxidation rate, was not affected by the amount of porosity and the size of the pores. This opens the possibility of using Cr<sub>2</sub>AlC foams in applications at high temperatures that requires high surface areas with excellent oxidation resistance, such as heat exchangers and catalyst supports.

### **3.3. Compressive strength of Cr<sub>2</sub>AlC foams**

Compressive strength of Cr<sub>2</sub>AlC foams containing 53 vol.% and 75 vol.% of porosity, and pore size between 180 and 250  $\mu$ m were measured before and after an oxidation treatment at 1200 °C during 1 h in air. Representative compression stress – displacement curves for 53 vol.% and 75 vol.% are shown in Figure 10a and 10b, respectively, meanwhile the mean values of the compressive strength with the standard deviations are shown in Table I. The stress – displacement curve for the Cr<sub>2</sub>AlC containing 53 vol.% of porosity shows 3 different regions. First, an initial linear phase is observed, which corresponds with an elastic behavior and maximal compression strength of 73 MPa. Afterwards, the curve is characterized by a plateau due to the progressive collapse of the porous structure. This is the typical compressive behavior of a ceramic foam,<sup>24</sup> which is totally different than the observed for dense and low porous ceramic materials, where a sudden failure typically occurs. The reason is related with the consecutive failure of single struts, avoiding the sudden failure of the system because the load is

sustained by the remaining struts. During this stage the compression strength of the  $\text{Cr}_2\text{AlC}$  foam steadily decreased from 73 MPa to 50 MPa. Finally, the porous structure totally collapsed after a displacement of more than 1 mm, which corresponds with > 10 % of the initial length of the sample. However, the stress – displacement curve is different when the 53 vol.% porous structure is previously oxidized at 1200 °C (Fig. 10a). The main difference resides in the maximal compressive strength, 127 MPa, which is significantly larger than without any oxidation. Nevertheless, the behavior of the curve is relatively similar. First, the characteristic elastic behavior is recorded up to the maximal strength, followed by a small plateau, a progressive smooth collapse of the structure and an abrupt collapse at the end. For the oxidized foam, the absorption of energy is much large since acceptable values of stress, around 60 MPa, are maintained from a displacement from 0.5 mm to 2.1 mm. Similar compressive behavior of the 75 vol.% porous foams with and without oxidation was identified. Reasonably, the compressive strength values were lower since the porosity increased. The  $\text{Cr}_2\text{AlC}$  foam with 75 vol.% porosity and no oxidation presented the characteristic curve for highly porous ceramic compounds. The maximal compressive strength was 13 MPa, and it was maintained practically constant during the whole test. The oxidized foams exhibited again larger values than the structure without any oxidation. The maximal compressive strength was 24 MPa, which is steadily decreased after a displacement of approx. 1.5 mm.

As the oxidized foams showed higher compressive strength, fracture surfaces after the mechanical tests of as prepared and oxidized foams containing 53 vol.% of porosity were analyzed in the SEM (Fig. 11). The fracture surfaces of the foam without oxidation show the collapse of the struts between the pores (Fig 11a). Intergranular fracture mode (Fig. 11b) was identified as main mechanism, where some grains presented reinforced mechanisms such as delamination and kink bands (Fig. 11c). However, the fracture surface of the oxidized foam is totally different. First, the outer  $\alpha\text{-Al}_2\text{O}_3$  layer and the intermediate carbide layer can be easily observed on the  $\text{Cr}_2\text{AlC}$  substrate. Both layers are continuous and follow

perfectly the outline of the pores. Furthermore, and this is advantageous for the compressive strength and the mechanical stability of the foams, the adhesion between these layer and the  $\text{Cr}_2\text{AlC}$  substrate is excellent, since no cracks and/or delamination at the interface were detected after the compression tests. Interestingly, the fracture mode of the  $\text{Cr}_2\text{AlC}$  is modified, as transgranular fracture mode became the main mechanism (Fig. 11d and e). The change of the fracture mode after the oxidation process is not still clear and more research is required, but it might be correlated with the tension stress that the  $\text{Cr}_2\text{AlC}$  grains suffered due to the CTE mismatch.  $\text{Cr}_2\text{AlC}$  presents larger thermal expansion ( $13.3 \times 10^{-6} \text{ K}^{-1}$ ) than  $\alpha\text{-Al}_2\text{O}_3$  ( $9.6 \times 10^{-6} \text{ K}^{-1}$ ),  $\text{Cr}_3\text{C}_2$  ( $10.3 \times 10^{-6} \text{ K}^{-1}$ ) and  $\text{Cr}_7\text{C}_3$  ( $10.0 \times 10^{-6} \text{ K}^{-1}$ ) so the  $\text{Cr}_2\text{AlC}$  grains are under tension. The  $\text{Cr}_2\text{AlC}$  grains are based on layered structures, as all the MAX phases, so when transgranular mode is the main mechanisms reinforced mechanisms are promoted. This modification from intergranular to transgranular is assumed to be the main responsible of the better compressive strength of the oxidized foams in comparison with the un-oxidized porous structures.

$\text{Cr}_2\text{AlC}$  foams show similar compressive strength than other advanced ceramic compounds containing the same amount of porosity, such as  $\text{Al}_2\text{O}_3$ ,<sup>24,25</sup>  $\text{ZrO}_2$ ,<sup>26</sup>  $\text{ZrB}_2$ ,<sup>27,28</sup> hydroxyapatite<sup>26</sup> and  $\text{SiC}$ <sup>29,30,31,32</sup> (Fig. 12). It should be noted that the pore size of these foams is different –sometimes larger and sometimes smaller –, and it has a critical effect on the compressive strength. Commonly, as smaller is the pore size, the strength of the foams is higher. Nevertheless, a clear tendency is observed. The  $\text{Cr}_2\text{AlC}$  foams present similar compressive strength than these advanced ceramics, improvement that is strongly enhanced when the  $\text{Cr}_2\text{AlC}$  foams are oxidized. Unfortunately, this is the first time that compressive strength of MAX phases containing high porosity (up to 75 vol.%) has been measured so comparison is not possible. Besides, to the best of our knowledge, this is also the first time that compressive strength has been characterized after an oxidation process, thus the increment in the mechanical response and the effect of the  $\alpha\text{-Al}_2\text{O}_3$  layer cannot be neither compared and/or correlated. However, the great potential of  $\text{Cr}_2\text{AlC}$  foams, and probably of other MAX phases containing aluminum as “A” atom, has

been demonstrated due to the excellent oxidation resistance, the better mechanical performance than other advanced ceramics, and the superior compressive strength after an oxidation treatment at high temperature. Therefore, this investigation clearly opens the possibility to use Cr<sub>2</sub>AlC foams to several applications at high temperatures such as heat exchangers and catalyst supports, although more investigation is absolutely required. Some investigations about long experiments under realistic conditions and thermal shock are carrying out by some of the authors, but deeper research about the response at high temperature of the foams is essential prior to define some particular application. Finally, it has to be highlighted that these Cr<sub>2</sub>AlC porous probes have been successfully manufactured by EDM despite their small dimensions and high content of porosity. Manufacturing of advanced ceramics is one of the major concerns to produce complex ceramic parts, and this problem is magnified when the components contain large amount of porosity. Here, we have demonstrated that highly porous MAX phases can be easily machined, which might reduce the final cost of MAX phase components.

## Conclusions

Cr<sub>2</sub>AlC foams with low (35 vol.%), intermediate (53 vol.%) and high (75 vol.%) porosity, and pore sizes between 90 and 400 µm were successfully processed by the sacrificial template technique using NH<sub>4</sub>HCO<sub>3</sub> as pore former. The developed foams showed a homogeneous distribution of the pores which were separated by struts with thicknesses around 10 – 60 µm. The foams were not significantly oxidized up to 800 °C, and further temperatures promoted the *in-situ* formation of an outer continuous protective α-Al<sub>2</sub>O<sub>3</sub> layer. This outer α-Al<sub>2</sub>O<sub>3</sub> layer protected against further oxidation up to 1300 °C, and is formed due to the preferential migration towards the surface of aluminum atoms from the Cr<sub>2</sub>AlC crystal structure. The aluminum atom migration causes the formation of an intermediate layer based on carbides, mainly Cr<sub>7</sub>C<sub>3</sub> and Cr<sub>3</sub>C<sub>2</sub>, between the alumina layer and the Cr<sub>2</sub>AlC bulk material. The adhesion between the different layers and the bulk material is excellent without any observation of spallation or

cracks up to 1300 °C, even when the external surfaces present sharp angles due to the curvature of the pores. The compressive strength of the Cr<sub>2</sub>AlC foams containing 53 and 75 vol.% of porosity and pore size between 180 - 250 µm were 73 MPa and 13 MPa, respectively. The compressive strength significantly increased when the foams were oxidized at 1200 °C during 1 h. The improvement is caused by switch from intergranular to transgranular fracture mode after the oxidation and it could be related to the formation of the α-Al<sub>2</sub>O<sub>3</sub> and the consequent CTE mismatch with the Cr<sub>2</sub>AlC substrates. These results open the possibility to use Cr<sub>2</sub>AlC foams in applications at high temperature under air conditions such as heat exchangers and catalyst supports.

### Acknowledgement

This work has been funded by the Germany's Federal Ministry of Education and Research ("Bundesministerium für Bildung und Forschung") under the MAXCOM project (03SF0534). The authors gratefully thank Dr. Doris Sebold from Forschungszentrum Jülich for her valuable assistance during the SEM analysis, as well as Mr. Witold Hildebrandt from RWTH Aachen for his precise work during the mechanical characterization.

### References

- <sup>1</sup> A.R. Studart, U.T. Gonzenbach, E. Tervoort, and L.J. Gauckler, "Processing routes to macroporous ceramics: A review," *J. Am. Ceram. Soc.*, **89** [6] 1771–1789 (2006).
- <sup>2</sup> A. Sommers, Q. Wang, X. Han, C. T'Joel, Y. Park, and A. Jacobi, "Ceramics and ceramic matrix composites for heat exchangers in advanced thermal systems—A review," *Appl. Therm. Eng.*, **30** [11–12] 1277–1291 (2010).
- <sup>3</sup> M.W. Barsoum, *MAX Phases. Properties of Machinable Ternary Carbides and Nitrides*. Wiley VCH, 2013.

- <sup>4</sup> B.M. Radovic and M.W. Barsoum, "MAX phases : Bridging the gap between metals and ceramics," *Am. Ceram. Soc. Bull.*, **92** [3] 20–27 (2013).
- <sup>5</sup> M.W. Barsoum and M. Radovic, "Elastic and Mechanical Properties of the MAX Phases," *Annu. Rev. Mater. Res.*, **41** [1] 195–227 (2011).
- <sup>6</sup> H. Li, S. Li, and Y. Zhou, "Cyclic thermal shock behaviour of a Cr<sub>2</sub>AlC ceramic," *Mater. Sci. Eng. A*, **607** 525–529 (2014).
- <sup>7</sup> S. Li, H. Li, Y. Zhou, and H. Zhai, "Mechanism for abnormal thermal shock behavior of Cr<sub>2</sub>AlC," *J. Eur. Ceram. Soc.*, **34** [5] 1083–1088 (2014).
- <sup>8</sup> Z.J. Lin, M.S. Li, J.Y. Wang, and Y.C. Zhou, "High-temperature oxidation and hot corrosion of Cr<sub>2</sub>AlC," *Acta Mater.*, **55** [18] 6182–6191 (2007).
- <sup>9</sup> J. Kašpar, P. Fornasiero, and N. Hickey, "Automotive catalytic converters: Current status and some perspectives," *Catal. Today*, **77** [4] 419–449 (2003).
- <sup>10</sup> M. Skoglundh and E. Fridell, "Strategies for enhancing low-temperature activity," *Top. Catal.*, **28** [April] 79–87 (2004).
- <sup>11</sup> T.R. Pollock and S. Tin, "Nickel based superalloys for advanced turbine engines: chemistry, microstructure and properties," *J. Propuls. power*, **22** [2] 361–374 (2006).
- <sup>12</sup> P. Colombo, "Conventional and novel processing methods for cellular ceramics.," *Philos. Trans. A. Math. Phys. Eng. Sci.*, **364** [1838] 109–124 (2006).
- <sup>13</sup> C. Hu, H. Zhang, F. Li, Q. Huang, and Y. Bao, "New phases' discovery in MAX family," *Int. J. Refract. Met. Hard Mater.*, **36** 300–312 (2013).

- <sup>14</sup> Z. Sun, A. Murugaiah, T. Zhen, A. Zhou, and M. Barsoum, "Microstructure and mechanical properties of porous Ti<sub>3</sub>SiC<sub>2</sub>," *Acta Mater.*, **53** [16] 4359–4366 (2005).
- <sup>15</sup> L. Hu, R. Benitez, S. Basu, I. Karaman, and M. Radovic, "Processing and characterization of porous Ti<sub>2</sub>AlC with controlled porosity and pore size," *Acta Mater.*, **60** [18] 6266–6277 (2012).
- <sup>16</sup> B. Velasco, E. Gordo, and S.A. Tsipas, "MAX phase Ti<sub>2</sub>AlC foams using a leachable space-holder material," *J. Alloys Compd.*, **646** 1036–1042 (2015).
- <sup>17</sup> C.R. Bowen and T. Thomas, "Macro-porous Ti<sub>2</sub>AlC MAX-phase ceramics by the foam replication method," *Ceram. Int.*, **41** [9] 12178–12185 (2015).
- <sup>18</sup> Z. Sun, Y. Liang, M. Li, and Y. Zhou, "Preparation of reticulated MAX-phase support with morphology-controllable nanostructured ceria coating for gas exhaust catalyst devices," *J. Am. Ceram. Soc.*, **93** [9] 2591–2597 (2010).
- <sup>19</sup> M. Potoczek, E. Guzi de Moraes, and P. Colombo, "Ti<sub>2</sub>AlC foams produced by gel-casting," *J. Eur. Ceram. Soc.*, **35** [9] 2445–2452 (2015).
- <sup>20</sup> J. Gonzalez-Julian, S. Onrubia, M. Bram, and O. Guillon, "Effect of sintering method on the microstructure of pure Cr<sub>2</sub>AlC MAX phase ceramics," *J. Ceram. Soc. Japan*, (2016).
- <sup>21</sup> Z. Sun, H. Hashimoto, W. Tian, and Y. Zou, "Synthesis of the MAX Phases by Pulse Discharge Sintering," *Int. J. Appl. Ceram. Technol.*, **7** [6] 704–718 (2010).
- <sup>22</sup> C.L. Zhou, T.W.L. Ngai, L. Lu, and Y.Y. Li, "Fabrication and characterization of pure porous Ti<sub>3</sub>SiC<sub>2</sub> with controlled porosity and pore features," *Mater. Lett.*, **131** 280–283 (2014).
- <sup>23</sup> D.B. Lee and T.D. Nguyen, "Cyclic oxidation of Cr<sub>2</sub>AlC between 1000 and 1300°C in air," *J. Alloys Compd.*, **464** [1–2] 434–439 (2008).

- <sup>24</sup> S. Meille, M. Lombardi, J. Chevalier, and L. Montanaro, "Mechanical properties of porous ceramics in compression : On the transition between elastic , brittle , and cellular behavior," *J. Eur. Ceram. Soc.*, **32** [15] 3959–3967 (2012).
- <sup>25</sup> J.S. Magdeski, "The porosity dependence of mechanical properties of sintered alumina," *J. Univ. Chem. Technol. Metall.*, **45** [2] 143–148 (2010).
- <sup>26</sup> H. Kim, S. Lee, C. Bae, Y. Noh, H. Kim, H. Kim, and J. Seung, "Porous ZrO<sub>2</sub> bone scaffold coated with hydroxyapatite with fluorapatite intermediate layer," *Biomaterials*, **24** 3277–3284 (2003).
- <sup>27</sup> E. Landi, D. Sciti, C. Melandri, and V. Medri, "Ice templating of ZrB<sub>2</sub> porous architectures," *J. Eur. Ceram. Soc.*, **33** 1599–1607 (2013).
- <sup>28</sup> V. Medri, M. Mazzocchi, and A. Bellosi, "ZrB<sub>2</sub> -Based Sponges and Lightweight Devices," *Int. J. Appl. Ceram. Technol.*, **8** [4] 815–823 (2011).
- <sup>29</sup> J. Eom, Y. Kim, I. Song, and H. Kim, "Processing and properties of polysiloxane-derived porous silicon carbide ceramics using hollow microspheres as templates," *J. Eur. Ceram. Soc.*, **28** 1029–1035 (2008).
- <sup>30</sup> J.-H. Eom and Y.-W. Kim, "Effect of additive composition on microstructure and strength of porous silicon carbide ceramics," *J. Mater. Sci.*, **44** 4482–4486 (2009).
- <sup>31</sup> J. Eom, Y. Kim, and S. Raju, "Processing and properties of macroporous silicon carbide ceramics : A review," *J. Asian Ceram. Soc.*, **1** [3] 220–242 (2013).
- <sup>32</sup> V. Medri and A. Ruffini, "Alkali-bonded SiC based foams," *J. Eur. Ceram. Soc.*, **32** 1907–1913 (2012).

## Figure caption

Figure 1. Characterization of the  $\text{Cr}_2\text{AlC}$  starting powder by a) XRD and b) and c) SEM.

Figure 2. Overall porosity as a function of the space holder content for the three different ranges of pore size distribution sintered at 1250 °C during 5h in Ar.

Figure 3. SEM micrographs of the polished surfaces with porosity and pore size of: a) 35 vol.% and 90-180  $\mu\text{m}$ , b) 53 vol. % and 180-250  $\mu\text{m}$  and c) 75 vol.% and 250-400  $\mu\text{m}$ .

Figure 4. SEM micrographs of the fracture surface of  $\text{Cr}_2\text{AlC}$  samples with 53 vol.% porosity and 180-250  $\mu\text{m}$  pore size.

Figure 5. TGA curve for the oxidation of  $\text{Cr}_2\text{AlC}$  material with 11 % porosity at a heating rate of 10 °C · min<sup>-1</sup> in air.

Figure 6. XRD on the surface of  $\text{Cr}_2\text{AlC}$  samples after oxidation at 800, 900, 1000, 1100, 1200 and 1300 °C for 1 h.

Figure 7. Cross sections of  $\text{Cr}_2\text{AlC}$  samples oxidized for 1 h at a) 1000 °C, b) 1100 °C, c) 1200 °C and d) 1300 °C.

Figure 8. a) Cross section of  $\text{Cr}_2\text{AlC}$  oxidized at 1300 °C, and EDS maps for b) Al, and c) Cr.

Figure 9. Cross section of the oxidized porous structures at a) 1000 °C, b) 1100 °C and c) 1300 °C.

Figure 10. Representative compression stress-crosshead displacement curves before and after the oxidation treatment at 1200 °C of  $\text{Cr}_2\text{AlC}$  samples with: a) 53 vol.% porosity, and b) 75 vol.% porosity

Figure 11. SEM micrographs of the fracture surfaces after the compression test of  $\text{Cr}_2\text{AlC}$  samples with 53 vol.% porosity and 180-250  $\mu\text{m}$  pore size for: a), b) and c) without oxidation, and d), e) and f) after oxidation at 1200 °C.

Figure 12. Compressive strength as a function of porosity for different advanced ceramic materials. Data points are labeled with their corresponding reference numbers.